Early winter barium excess in the Southern Indian Ocean as an annual remineralisation proxy (GEOTRACES GIPr07 cruise)

Natasha René van Horsten[1,2,3], Hélène Planquette[1], Géraldine Sarthou[1], Thomas James Ryan-Keogh[2], Thato Nicholas Mtshali[4], Alakendra Roychoudhury[3], and Eva Bucciarelli[1]

[1]Univ Brest, CNRS, IRD, Ifremer, LEMAR, F-29280 Plouzane, France.
[2]SOCCO, CSIR, Lower Hope road, Cape Town, South Africa, 7700.
[3]TracEx, Department of Earth Sciences, Stellenbosch University, Stellenbosch, South Africa, 7600.
[4]Department of Environment, Forestry and Fisheries, Oceans and Coast, Foretrust Building, Martin Hammerschlag Way, Cape Town, South Africa, 8001

Correspondence to: Natasha van Horsten (nvhorsten@csir.co.za), Eva Bucciarelli (Eva.Bucciarelli@univ-brest.fr)

Abstract. The Southern Ocean is of global importance and processes such as mesopelagic remineralisation that impact the efficiency of the biological carbon pump in this region is of substantial interest. During this study the proxy barium excess which is utilised to shed light on mesopelagic remineralisation was measured at seven stations along 30°E in the Southern Indian Ocean during early austral winter of 2017. To our knowledge this is the first reported winter study utilising this proxy in the Southern Ocean. Concentrations of 59 to 684 pmol L^{-1} were comparable to those observed throughout other seasons, indicating that this proxy has a longer timescale than previously thought. Background barium excess values observed in deep waters were also similar to previous studies, not having declined down to an expected "true" Southern Ocean background value. It is apparent that processes driving the mesopelagic barium excess signal are still underway during early winter. Indicating that continuous remineralisation is sustained at levels comparable to summer, well after bloom termination. Moreover, linking integrated remote sensing primary production to the mesopelagic barium excess signal reiterates a longer timescale. The significant positive correlations obtained in the Antarctic and Subantarctic zones suggest that mesopelagic barium excess stock can be used as a remineralisation proxy on an annual timescale and possible inference of carbon remineralisation from remote sensing data on an annual and basin scale.

1   Introduction

The Southern Ocean (SO) is a carbon sink of global significance responsible for 40 – 50 % of the global oceans' carbon uptake (Friedlingstein et al., 2019; Gregor et al., 2019; Gruber et al., 2019). Oceanic carbon uptake is regulated by various processes, including the biological carbon pump (BCP). The pathway by which inorganic carbon is consumed and released by photosynthetic organisms through photosynthesis and respiration (Sarmiento and Gruber, 2006), thereby regulating the earth's carbon cycle by partially sequestering photosynthetically fixed CO_2 in the ocean interior (Honjo et al., 2014). In particular, the

30   SO BCP is a crucial contributor to the earth's carbon cycle by exporting, from surface waters, ~ 3 Pg C yr^{-1} of the ~ 10 Pg C

31   yr^{-1} global export production (Schlitzer, 2002). The efficiency of the BCP is linked to the export and preservation of surface

32   particulate matter and is directly linked to atmospheric CO_2 levels, on glacial-interglacial timescales (Honjo et al., 2014;

33   Sigman et al., 2010).

34   Sedimentation out of the surface layer (~100 m) is defined as surface export and out of the mesopelagic zone (~1000 m) as

35   deep export (Passow and Carlow, 2012). There are large gaps in our knowledge with regard to deep carbon export, internal

36   cycling and the seasonality of these processes (Takahashi et al., 2012). The magnitude of deep carbon export is dependent on

37   the efficiency of mesopelagic remineralisation (Jacquet et al., 2015) which can balance or even exceed particulate organic

38   carbon (POC) surface export, especially later in the growing season, thereby limiting deep export (Buesseler and Boyd, 2009;

39   Cardinal et al., 2005; Jacquet et al., 2011, 2015; Lemaitre et al., 2018; Planchon et al., 2013). A possible explanation for

40   imbalances between surface export and mesopelagic processes can be lateral advection of surface waters with lower particle

41   export relative to the mesopelagic signal (Planchon et al., 2013). It is also possible that continued remineralisation of earlier

42   larger export fluxes is detected in the mesopelagic signal but not in the export fluxes of in situ observations (Planchon et al.,

43   2013). In addition to this, the efficiency of remineralisation is influenced by the size and composition of exported particles

44   (Rosengard et al., 2015; Twining et al., 2014) as well as the pathway by which these particles are transported downwards (e.g.,

45   eddy-subduction, active migration, sinking or mixing) from the surface mixed layer to the mesopelagic zone (Boyd et al., 2019;

46   Le Moigne, 2019), creating an intricate web of processes to disentangle. Mesopelagic remineralisation has also been shown to

47   be influenced by environmental factors, such as temperature, phytoplankton community structure and nutrient availability

48   (Bopp et al., 2013; Buesseler and Boyd, 2009). Indeed, nutrient limitation in surface waters limits export and consequently

49   mesopelagic remineralisation by promoting the shift to smaller phytoplankton assemblages that preferentially take up recycled

50   nutrients in the surface mixed layer (Planchon et al., 2013). Phytoplankton community composition exerts an important control

51   where diatoms are more efficiently exported, due to their large size and ballasting by biogenic silica, compared to smaller non-

52   diatom phytoplankton (Armstrong et al., 2009; Buesseler, 1998; Ducklow et al., 2001). Latitudinal trends in remineralisation

53   efficiency can also be linked to temperature-dependent heterotrophs that are responsible for remineralisation (DeVries and

54   Weber, 2017; Marsay et al., 2015). The mesopelagic layer is under-studied, especially in the high latitudes, and therefore these

55   processes are poorly constrained, despite their importance to global elemental cycles, including that of carbon (Le Moigne,

56   2019; Robinson et al., 2010).

57   Export and remineralisation tracers, such as ^{234}Th/^{238}U and apparent oxygen utilisation (AOU), have been used to study

58   mesopelagic POC remineralisation fluxes (Buesseler et al., 2005; Planchon et al., 2013; Lemaitre et al., 2018). Excess ^{234}Th

59   activities are used to measure surface export and ^{234}Th/^{238}U ratios higher than 1 are attributed to remineralisation, integrating

60   processes over a 2 to 3 week period (Buesseler et al., 2005; Planchon et al., 2013). AOU is the depletion of oxygen (O_2) in the

61   ocean interior, relative to surface saturation, due to biological respiration, when surface water masses are subducted. AOU is

62   dependent on salinity and temperature and integrates remineralisation on timescales of years to decades (Ito et al., 2004).

63 Inaccuracies have, however, been detected with AOU as a remineralisation proxy, specifically in high latitude areas, due to O_2

64 undersaturation as a consequence of large temperature gradients (Ito et al., 2004).

65 Barium excess (Ba_{xs}) is another proxy utilized to yield estimates of mesopelagic POC remineralisation fluxes. It is defined as

66 the "biogenic" portion of particulate Barium (pBa) as barite crystals, formed by the decay of bio-aggregates below the surface

67 mixed layer (Bishop, 1988; Dehairs et al., 1997; Lam and Bishop, 2007; Legeleux and Reyss, 1996; van Beek et al., 2007). As

68 these crystals are released a Ba_{xs} peak is formed within the mesopelagic zone which has been found to correlate to primary

69 production (PP), O_2 consumption and POC remineralisation (Dehairs et al., 1997). Depth-integrated rates of O_2 consumption

70 between the base of the mixed layer and 1000 m were estimated using an inverse 1-D advection-diffusion-consumption model

71 (Shopova et al., 1995) to develop a transfer function between the Ba_{xs} signal and the rate of surface POC export for subsequent

72 mesopelagic remineralisation (Dehairs et al., 1997). Strong correlations have been obtained between the well-established

73 export/remineralisation flux proxy [234]Th and Ba_{xs}, during studies conducted in the SO and the North Atlantic, confirming the

74 validity of Ba_{xs} as a remineralisation proxy (Cardinal et al., 2005; Lemaitre et al., 2018; Planchon et al., 2013). Estimates of

75 POC remineralisation fluxes, using the Ba_{xs} proxy, are directly influenced by the background signal of Ba_{xs}, after partial

76 dissolution and sedimentation from the previous bloom season, which can be thought of as the "pre-formed Ba_{xs}", defined as

77 the $Ba_{residual}$ signal at zero O_2 consumption (Jacquet et al., 2015). Studies conducted in spring and summer suggest that the

78 mesopelagic Ba_{xs} signal lasts between a few days to a few weeks (Dehairs et al., 1997; Cardinal et al., 2005; Jacquet et al.,

79 2007, 2008a).

80 Winter Ba_{xs} data is thus crucial for giving insight into the true SO $Ba_{residual}$ values (Jacquet et al., 2008b, 2011) and the timescale

81 of the mesopelagic Ba_{xs} signal, which we believe to be longer than a few weeks. In this context, as part of a GEOTRACES

82 process study (GIpr07) of a transect along 30°E in the Southern Indian Ocean (SIO, 58.5°S to 41.0°S), we studied Ba_{xs}

83 distributions during early austral winter (July 2017) to better constrain the SO $Ba_{residual}$ concentrations and the timescale of this

84 proxy. We also aim to better understand the seasonal cycle and how it links to PP on a basin scale.

85 ## 2   Materials and Methods

86 ### 2.1   Sampling and hydrography

87 During the GEOTRACES GIpr07 cruise, which took place in early austral winter (28 June - 13 July 2017) onboard the R/V

88 *SA Agulhas II*, seven stations were sampled along 30°E, from 58.5°S to 41.0°S (WOCE I06S, Figure 1a). At each station

89 between 15 and 21 samples were collected from 25 m down to 1500 m, for shallow stations, and down to 4250 m, for deep

90 stations, to be analysed for multiple parameters.

91 Positions of the fronts during the cruise were determined using mean absolute dynamic topography data from the CLS/AVISO

92 product (Rio et al., 2011), with boundary definitions from Swart et al. (2010). From north to south the fronts are, the Subtropical

93 Front (STF), the Subantarctic Front (SAF), the Polar Front (PF), the Southern Antarctic Circumpolar Front (SACCf) and the

94 Southern Boundary (SBdy) (Figure 1a).
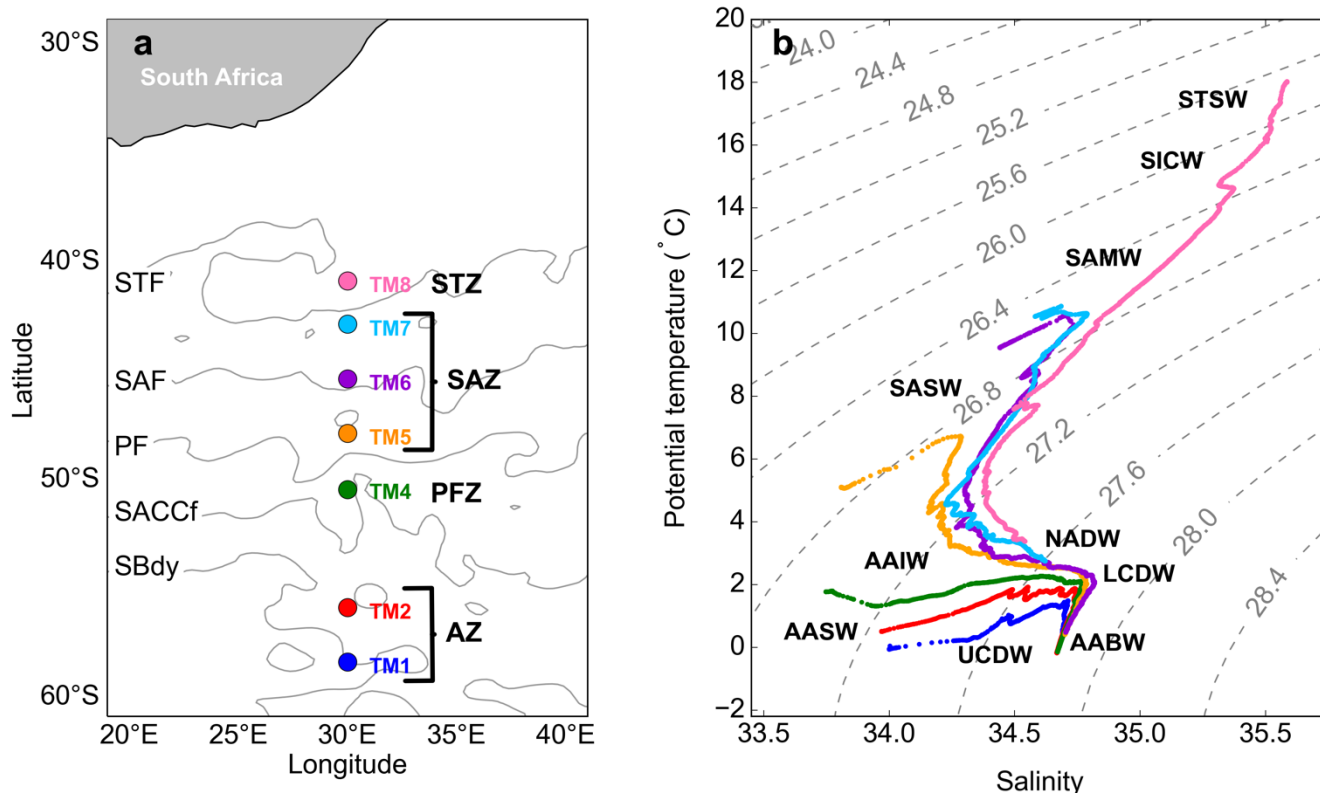
Figure 1: (a) GEOTRACES GIPr07 cruise sampling stations overlaid on a map with frontal positions; namely, the Subtropical Front (STF), the Subantarctic Front (SAF), the Polar Front (PF), the Southern Antarctic Circumpolar Front (SACCf) and the Southern Boundary (SBdy), as determined by mean absolute dynamic topography (MADT) and crossing over three zones; namely, the Antarctic zone (AZ), the Polar frontal zone (PFZ), the Subantarctic zone (SAZ) and the Subtropical zone (STZ), **(b)** Potential temperature plotted against salinity, overlaid on isopycnals and identification of water masses sampled; namely, Subtropical Surface Water (STSW), South Indian Central Water (SICW), Subantarctic Mode Water (SAMW), Subantarctic Surface Water (SASW), Antarctic Intermediate Water (AAIW), Antarctic Surface Water (AASW), North Atlantic Deep Water (NADW), Lower Circumpolar Deep Water (LCDW), Upper Circumpolar Deep Water (UCDW), Antarctic Bottom Water (AABW).

2.2 Temperature, salinity and dissolved O₂

Temperature (°C), salinity and dissolved O_2 (µmol L^{-1}) profiles were measured by sensors (SBE 911plus). At each cast discrete seawater samples were collected for analysis and calibration of the sensor data. Discrete samples were analysed onboard for salinity (8410A Portasal salinometer) and dissolved O_2 concentrations (Metrohm 848 titrino plus; Ehrhardt et al., 1983). Strong correlations were obtained between sensor data and discrete samples for salinity ($R^2 = 0.99$) and dissolved O_2 ($R^2 = 0.83$), validating the sensor data which was then used for further data interpretation. Temperature and salinity measurements were used to calculate potential density (σ_θ), using the python seawater package (Gill, 1982), to characterise water masses sampled. The σ_θ profiles were also used to identify the mixed layer depth (MLD) at all stations during the cruise, which was defined as the depth at which there is a change of 0.03 kg m^{-3} in σ_θ from a near-surface value at 10 m depth (de Boyer Montégut, et al., 2004).

2.3   pBa and pAl

Profile sampling of the water column was conducted with a GEOTRACES compliant trace metal clean CTD housed on an epoxy coated aluminium frame rosette with titanium bolts equipped with 24 x 12 L trace metal clean Teflon coated GO-FLO bottles (General Oceanics). All sampling and analyses were conducted following the GEOTRACES clean sampling and analysis protocols (Cutter et al. 2017). Volumes of 2 to 7 L of seawater were filtered from the GO-FLO bottles onto acid-washed polyethersulfone filters (25 mm diameter, Supor, 0.45 µm pore size), mounted on swinnex filter holders, for pBa and pAl analyses. After filtration, filters were placed in trace metal clean petri slides (Pall) and kept frozen at -20°C until further processing on land. Sample processing was conducted under a class 100 HEPA filtered laminar flow and extraction hood in a clean laboratory.

The pBa and pAl samples were processed and analysed 6 months after sample collection at LEMAR (France). Filters containing the samples were acid reflux digested at 130°C in acid-cleaned savillex vials using a mixture of HF and HNO_3 (both Ultrapure grade, Merck) solutions (Planquette and Sherrell, 2012). Archive solutions were stored in 3 ml of 0.12 M HNO_3 (Ultrapur grade), of which 250 µL was diluted up to 2 mL for analysis by sector field inductively coupled plasma mass spectrometry (SF-ICP-MS, Element XR Thermo Scientific). Samples were spiked with 1 µg L^{-1} indium as an internal standard to correct for instrument drift. The detection limits, defined as three times the standard deviation of the blanks (unused filter blanks), were 0.39 pmol L^{-1} and 0.03 nmol L^{-1} (n = 5) for pBa and pAl, respectively. Three certified reference materials (BCR 414, MESS 4 and PACS 3) were processed and analysed with the samples to assess the accuracy of the methodology. Our values were in good agreement with the certified values of the reference materials (Table 1) (Jochum et al., 2007). Percentage error of analyses was determined by the repeat analysis of random samples during each run, the mean percentage error of sample analysis for pBa and pAl was 9.2 ± 2.5 % and 11.1 ± 4.6 % (mean ± SD, n = 6), respectively.

Table 1: Certified Reference Material recovery data for accuracy determination of pBa and pAl analyses

	pBa (mg/kg)	pAl (mg/kg)
PACS 3 certified (mean ± SD)		65800 ± 1700
PACS 3 measured (mean ± SD)		73156 ± 15416
PACS 3 mean % recovery		111 ± 23
MESS 4 certified	920	79000 ± 2000
MESS 4 (mean ± SD)	1033 ± 28	100048 ± 26870
MESS 4 mean % recovery ± SD	112 ± 3	127 ± 34
BCR 414 indicative values	32 ± 5	2384 ± 652
BCR 414 (mean ± SD)	34 ± 4	2651 ± 317

BCR 414 mean % recovery ± SD	105 ± 12	111 ± 13

35

2.4 Ba_{xs} as a proxy for mesopelagic POC remineralisation

Ba_{xs}, the non-lithogenic fraction of the total pBa, was calculated by subtracting the lithogenic fraction of pBa from the total pBa measured using Eq. 1. The lithogenic contribution to pBa was calculated by multiplying the pAl concentration with the Ba/Al upper continental crust (UCC) ratio, 0.00135, as determined by Taylor and McLennan (1985).

$$Ba_{xs} = [pBa] - ([pAl] \times (Ba/Al)_{UCC}) \qquad (1)$$

The mesopelagic POC remineralisation flux was estimated using Eq. 2 (Shopova et al., 1995; Dehairs et al., 1997).

$$Mesopelagic\ POC\ remineralisation = Z \times JO_2 \times (C{:}O_2)_{Redfield\ Ratio} \times 12.01 \qquad (2)$$

Where the mesopelagic POC remineralisation flux is expressed in mg C m^{-2} d^{-1}, Z is the depth range of the mesopelagic Ba_{xs} layer (100 - 1000 m), C:O_2 is the stoichiometric molar ratio of carbon to O_2 consumption by remineralisation as per the Redfield Ratio (127/175, Broecker et al., 1985), 12.01 is the molar mass of carbon (g mol^{-1}) and JO_2 is the rate of O_2 consumption (µmol L^{-1} d^{-1}) as estimated using Eq. 3.

$$JO_2 = (Mesopelagic\ Ba_{xs} - Ba_{residual})/17200 \qquad (3)$$

Where mesopelagic Ba_{xs} is the depth-weighted average (DWA) Ba_{xs} of the mesopelagic zone (pmol L^{-1}), the constant value of 17200 is the slope of the linear regression of DWA Ba_{xs} (pmol L^{-1}) versus O_2 consumption rate (µmol L^{-1} d^{-1}) using the SO transfer function by Dehairs et al. (1997) and $Ba_{residual}$ is the deep ocean background value of Ba_{xs} at zero oxygen consumption. The literature value of 180 pmol L^{-1} was used as the $Ba_{residual}$ value (Dehairs et al., 1997) in our calculations.

The $Ba_{residual}$ value for our study was calculated as the mean Ba_{xs} concentrations of samples below 2000 m, using the PF to divide the SO into two zones (north of the polar front (NPF) and south of the polar front (SPF)). The integrated mesopelagic Ba_{xs} stock (µmol m^{-2}) over the mesopelagic layer (100-1000 m) was calculated from the DWA Ba_{xs} in order to investigate the link between the accumulated mesopelagic signal and the corresponding integrated remote sensing PP.

2.5   Integrated remotely sensed PP

The integrated remote sensing PP (mg C m^{-2} d^{-1}) within the surface mixed layer was calculated using the CbPM algorithm (Behrenfeld et al., 2005), which requires chlorophyll (mg m^{-3}), particulate backscatter (λ 443 nm, m^{-1}), photosynthetically active radiation (PAR; µmol photons m^{-2} d^{-1}) and MLD (m). Ocean Colour Climate Change Initiative (OC-CCI) data (https://esa-oceancolour-cci.org/) which blends existing data streams into a coherent record meeting the quality requirements for climate assessment (Sathyendranath et al., 2019) were used for chlorophyll and particulate backscatter. PAR was taken from GLOB colour (http://www.globcolour.info/), and the MLD was taken from the climatology of de Boyer Montegut et al. (2004). The data were regridded to 0.25° spatially, using bilinear interpolation, and averaged monthly. The integrated CbPM

was averaged over a 6 x 1° rectangular sample area, positioned 6° upstream longitudinally, and 1° latitudinally centred around each sampled station (see discussion for details).

2.6   Integrated % POC remineralised

The integrated remineralised POC (mg C m^{-2}) was estimated by multiplying the POC remineralisation flux (mg C m^{-2} d^{-1}), as estimated using the Ba$_{xs}$ proxy method, by the number of days over which the corresponding remote sensing PP (mg C m^{-2} d^{-1}) was subsampled. The % POC remineralised was then estimated as the percentage of integrated remote sensing PP (mg C m^{-2}) remineralised, assuming that the mesopelagic Ba$_{xs}$ stock signal is due to the remineralisation of the integrated surface signal, for all available literature data and early winter data from this study.

2.7   Statistical analysis

For statistical analysis, the least squares regression method was applied for assessment of significant correlations (Barbur et al., 1994). Significant differences between zones and between regression slopes were tested using Welch's t-test, with an alpha of 0.05 (95 % confidence level) (Kokoska and Zwillinger, 2000).

3   Results

3.1   Hydrography

The potential temperature and salinity along the transect ranged from -0.06 to 18.03 °C and from 33.77 to 35.59, respectively. They define three hydrographic zones; namely, the Antarctic zone (AZ; $\theta < 2.5$ °C; $S \leq 34$) from 50°S to 58°S, the Subantarctic zone (SAZ; $5 < \theta < 11$ °C; $33.8 < S < 34.7$) between 43°S and 48°S, and the Subtropical zone (STZ; $\theta \geq 17.9$ °C; $S \cong 35.6$) at 41°S (Figure 1a; Anilkumar and Sabu, 2017; Orsi et al., 1995). The MLDs along the transect ranged between 97 and 215 m (144 ± 39 m; mean ± SD, n = 7), shoaling towards the PF (Table S1).

As can be observed on the T-S plot of stations sampled (Figure 1b), different water masses were sampled along the transect throughout the water column. SPF ($\gtrsim$50°S; TM1, 2 & 4), from surface to depth, Antarctic Surface Water (AASW; $27 < \sigma_\theta < 27.4$ kg.m^{-3}), Upper and Lower Circumpolar Deep Water (UCDW; $27.2 < \sigma_\theta < 27.75$ kg.m^{-3} and LCDW; $27.75 < \sigma_\theta < 27.85$ kg.m^{-3}, respectively), and Antarctic Bottom Water (AABW; $27.8 < \sigma_\theta < 27.85$ kg.m^{-3}) were characterized. NPF and south of the STF ($<$50°S; TM5, 6 & 7), from surface to depth, Subantarctic Surface Water (SASW; $26.5 < \sigma_\theta < 26.75$ kg.m^{-3}), Antarctic Intermediate Water (AAIW; $26.7 < \sigma_\theta < 27.4$ kg.m^{-3}), North Atlantic Deep Water (NADW; $27 < \sigma_\theta < 27.85$ kg.m$^{-3)}$ and, as far north as 45.5°S, AABW close to the ocean floor, were identified. At the northernmost station (TM8; 41°S) in the STZ, the water masses sampled include Subtropical Surface Water (STSW; $\sigma_\theta \cong 25.7$ kg.m^{-3}), South Indian Central Water (SICW; $25.8 < \sigma_\theta < 26.2$ kg.m^{-3}), Subantarctic Mode Water (SAMW; $26.2 < \sigma_\theta < 26.6$ kg.m^{-3}), AAIW and NADW.

3.2   Dissolved O$_2$

Dissolved O$_2$ concentrations ranged from 159 to 333 µmol L^{-1} (Figure 2). Maximum concentrations were observed in the surface mixed layer, increasing southwards along the transect, with a mean value of 287 ± 40 µmol L^{-1} (mean ± SD, n = 700). A decrease in concentrations below the MLD coincided with an increase in σ$_\theta$. SPF the decrease in dissolved O$_2$ concentrations at the MLD was sharp and relatively shallow when compared to profiles NPF, which were more gradual, spanning a wider depth range. Within the mesopelagic zone concentrations decreased down to 204 ± 29 µmol L^{-1} (mean ± SD, n = 6373), then remained relatively uniform below 1000 m at 192 ± 113 µmol L^{-1} (mean ± SD, n = 12950).
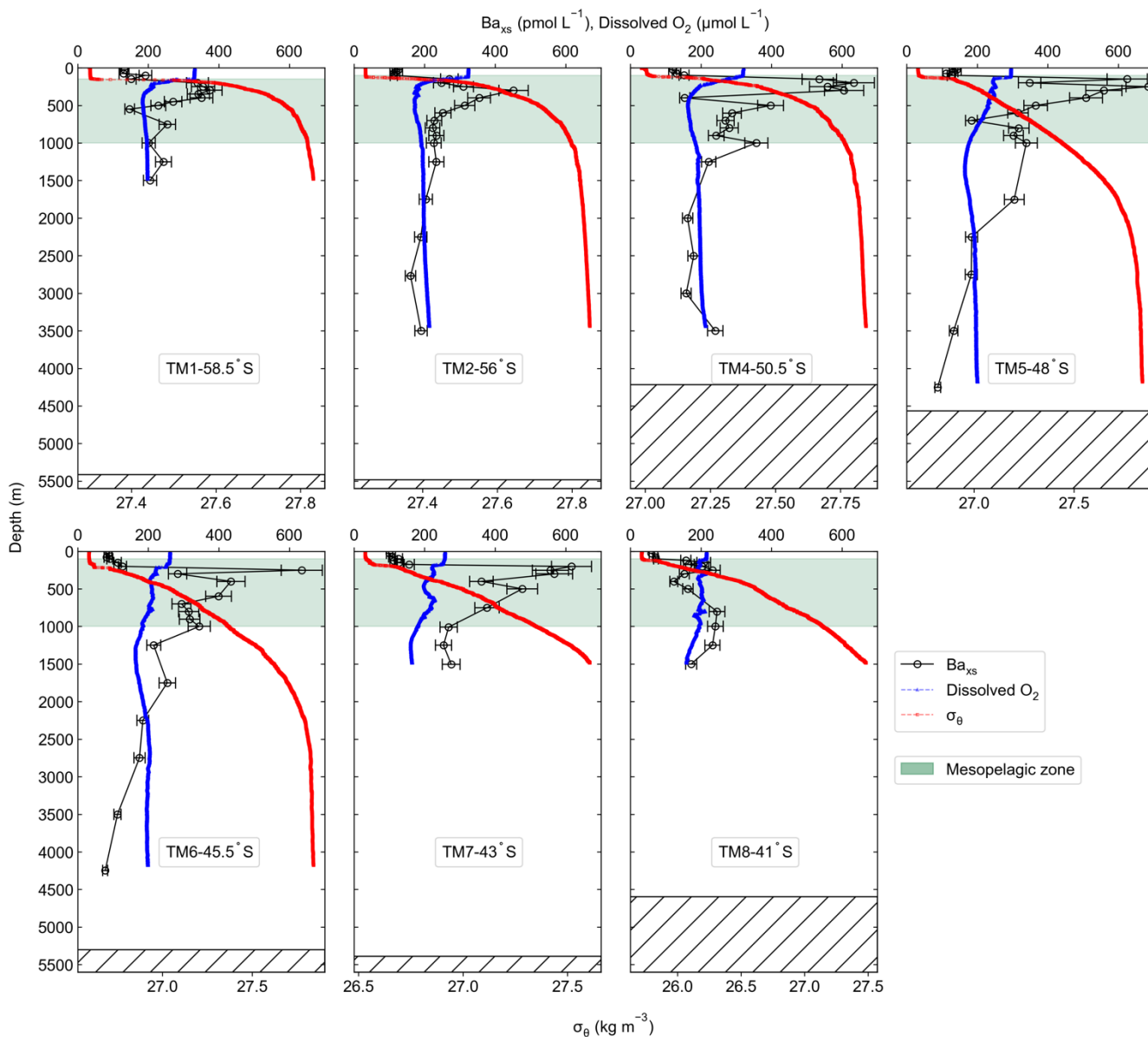
Figure 2: Ba$_{xs}$ (black circles) with error bars, potential density (red squares) and dissolved O$_2$ (blue triangles) profiles sampled along the transect, plotted against depth, for stations TM1 to TM8, from south to north. Green shaded area is the mesopelagic zone, and the hatched area is the ocean floor.

3.3   Ba$_{xs}$ and estimated POC remineralisation fluxes

Total pBa and Ba$_{xs}$ profiles were nearly identical with a mean percentage Ba$_{xs}$ to total pBa of 99 ± 1 % (mean ± SD, n = 124; Table S2), indicating that pBa from lithogenic sources was negligible, further supported by the lack of correlation between pAl and pBa (R^2 = 2 x 10^{-6}). This ensures the accurate estimation of Ba$_{xs}$, which requires that less than 50 % of pBa should be associated with lithogenic inputs (Dymond et al., 1992).

Ba_{xs} concentrations ranged from 59 to 684 pmol L^{-1}. All profiles exhibited a depletion of Ba_{xs} in the upper surface waters (59 - 152 pmol L^{-1}), then a rapid increase below the MLD (~150 m), with concentrations ranging between 113 and 684 pmol L^{-1} in the mesopelagic zone (100 - 1000 m, Figure 2). At the two southernmost stations (TM1 and TM2), mesopelagic Ba_{xs} peaks spanned a narrower depth range (100 - 600 m) than stations further north, with concentrations reaching values of ~ 400 pmol L^{-1}. In the polar frontal zone (PFZ) and the SAZ, where concentrations increased to a maximum of 684 pmol L^{-1} at 48°S (TM5), the subsurface increase of Ba_{xs} started at slightly deeper depths (150 - 200 m) and spanned wider depth ranges down to 1000 m. The STZ station, at 41°S (TM8), had the lowest concentrations, only increasing up to ~ 200 pmol L^{-1}. Double peaks were observed at all stations NPF, the shallow and more substantial peak occurring in the upper mesopelagic zone and a second peak in the lower mesopelagic zone. Below the mesopelagic zone, Ba_{xs} concentrations decreased down to ~ 180 pmol L^{-1} and remained somewhat uniform.

The $Ba_{residual}$ concentration of the southern part of the transect, SPF, was 183 ± 29 pmol L^{-1} (mean ± SD, n = 7), whereas the northern part of the transect, NPF, was 142 ± 45 pmol L^{-1} (mean ± SD, n = 8). The two zones were however not significantly different to each other when conducting Welch's t-test (t-statistic = 2.10; p-value = 0.06) and, when averaging all samples below 2000 m along the transect, the $Ba_{residual}$ concentration was 161 ± 43 pmol L^{-1} (mean ± SD, n = 15).

Estimated POC remineralisation fluxes ranged from 6 to 96 mg C m^{-2} d^{-1} (Table S1), increasing northwards from the southernmost station up to the PFZ from 32 to 92 mg C m^{-2} d^{-1}, then decreased down to 70 mg C m^{-2} d^{-1} at the SAF. The highest flux of 96 mg C m^{-2} d^{-1}, was estimated in the SAZ and the lowest flux was estimated in the STZ at 6 mg C m^{-2} d^{-1}.

3.4   Integrated % POC remineralised

The % POC remineralised of integrated remote sensing PP was split into two zones within the SO, SPF (19 ± 15 %; mean ± SD, n = 39) and NPF (25 ± 58 %; mean ± SD, n = 31; Table S1), with no significant difference (Welch's t-test; t-statistic = 0.54; p-value = 0.59).

4   Discussion

4.1   Early wintertime surface and mesopelagic Ba_{xs} and $Ba_{residual}$ values

When taking into account literature values, a noticeable difference between profiles sampled early in the bloom season (Dehairs et al., 1997; Jacquet et al., 2015) versus those sampled later (Cardinal et al., 2001; Planchon et al., 2013), are the contrasted concentrations of Ba_{xs} in the surface mixed layer early in the bloom season. Dehairs et al., (1997) have shown that these concentrations of Ba_{xs} can be as high as 9000 pmol L^{-1} in areas of high productivity during spring, which then becomes depleted to concentrations below the SO $Ba_{residual}$ value of ~ 180 pmol L^{-1}, as productivity declines and surface POC export increases (Planchon et al., 2013). These high surface concentrations are, however, not the same as that measured within the mesopelagic zone (Jacquet et al., 2011). Surface water concentrations are associated with Ba adsorbed onto particles whereas the mesopelagic Ba_{xs} signal is due to barite crystals formed within decaying bio-aggregates (Cardinal et al., 2005; Lam and Bishop,

239 2007; Lemaitre et al., 2018; Sternberg et al., 2005). In this study, we observed surface depletion of Ba_{xs} at all stations, in line

240 with the assumption that the bulk surface export from the preceding bloom had been achieved at the time of sampling and, the

241 majority of the Ba_{xs} had been transferred to the mesopelagic zone. This was in association with low surface chlorophyll α

242 concentrations, which ranged from 0.186 to 0.513 µg L^{-1} along the transect (Figure S1).

243 Sharp gradients in $σ_θ$ observed at the MLD, have previously been identified as the depth at which decaying bio-aggregates are

244 formed (Lam and Bishop, 2007). These gradients coincided with an increase in Ba_{xs} (Figure 2), linking the subsurface Ba_{xs}

245 signal to the decaying bio-aggregates as per previous studies (Cardinal et al., 2005; Dehairs et al., 1997; Jacquet et al., 2011).

246 Additionally, gradients observed in dissolved O_2 profiles along the transect are also accompanied by coinciding, opposite

247 gradients in Ba_{xs}, in line with O_2 consumption due to remineralisation within the mesopelagic zone (Figure 2) (Cardinal et al.,

248 2005; Jacquet et al., 2005, 2011). The observed range of mesopelagic Ba_{xs} concentrations (113 - 684 pmol L^{-1}) were comparable

249 to those previously reported in SO open waters (~ 200 - 1000 pmol L^{-1}; Cardinal et al., 2001, 2005; Jacquet et al., 2005, 2008a,

250 2008b, 2011, 2015; Planchon et al., 2013).

251 Ba_{xs} profiles exhibited similar distributions to those reported throughout bloom seasons in the SO, with distinct peaks observed

252 within the mesopelagic zone across all stations. Earlier in the bloom season peaks mostly occur within the upper half of the

253 mesopelagic zone (100 - 500 m) (Cardinal et al., 2001, 2005; Jacquet et al., 2005, 2008a, 2011, 2015), but as the season

254 progresses, they deepen down towards the bottom half of the mesopelagic zone (500 - >1000 m) (Jacquet et al., 2008b,

255 Planchon et al., 2013). Deepening and widening of the remineralisation depth range can be expected as the season progresses,

256 due to continued remineralisation taking place as particles sink to the bottom of the mesopelagic zone (Lemaitre et al., 2018;

257 Planchon et al., 2013). This is also what we observed during winter at stations NPF, with a second peak in deeper waters, as

258 observed by Jacquet et al. (2008b) during the iron (Fe) fertilization experiment (EIFEX). The deeper peak could also be linked

259 to relatively larger cells that sink faster as they remineralise, possibly a large bloom early in the season.

260 A distinct latitudinal trend in mesopelagic DWA Ba_{xs} has generally been observed in the SO with the highest values in the

261 PFZ, decreasing north and southwards from the PF. These latitudinal trends tend to be accompanied by a coinciding trend in

262 in situ surface biomass measurements (Cardinal et al., 2005; Dehairs et al., 1997, Jacquet et al., 2011; Planchon et al., 2013).

263 During our early winter study, we observed a similar latitudinal trend in mesopelagic Ba_{xs} stock (µmol m^{-2}), with an increase

264 from the southernmost station up to the PF, then varying around a maximum in the SAZ, down to the lowest value in the STZ,

265 whereas integrated PP increased exponentially northwards (Figure S1). Time of sampling and extended blooms, which are

266 characteristic of the SAZ (Thomalla et al., 2011), could be contributing factors to the higher values observed in PP and

267 mesopelagic Ba_{xs} distributions at stations NPF (Figure S1). Contrary to what was expected, the profiles observed during our

268 early winter study still show a significant mesopelagic remineralisation signal, well after the decline of the summer bloom,

269 which occurred between April and May, as defined by the point in time when community losses outweigh the growth rate

270 (Thomalla et al., 2011).

271 We did not observe the expected wintertime decline in the $Ba_{residual}$ signal to the "true" SO background values, when PP and

272 bacterial activity are minimal (Jacquet et al., 2011). A concentration of 180 pmol L^{-1} is considered the background value for

773 saturated waters SPF, whereas undersaturation of Ba_{xs} is expected in deep waters NPF, thereby resulting in lower background

774 values (Jacquet et al., 2011; Monnin et al., 1999; Planchon et al., 2013), this was, however, not observed during this early

775 winter study. The $Ba_{residual}$ concentrations NPF and SPF were not significantly different to each other and the mean $Ba_{residual}$

776 concentration along the whole transect was also not significantly different to the background value of 180 pmol L^{-1}, used in

777 previous studies (Dehairs et al. 1997; Jacquet et al., 2015; Planchon et al., 2013). We observed the lowest mesopelagic signal

778 in the STZ, where it is possible that the background values in the STZ could be much lower than 180 pmol L^{-1}, as it is considered

779 undersaturated (Monnin et al., 1999; Planchon et al., 2013). We did not, however, sample below 1500 m in this region and can

780 therefore not elaborate further on that. The winter background signal might never be achieved due to ongoing barite

781 precipitation and remineralisation, as well as the release of labile Ba, which is attached to phytoplankton as they decay,

782 precipitating into barite crystals, a process which could possibly continue throughout winter (Cardinal et al., 2005).

4.2   Timescale of the mesopelagic Ba_{xs} signal

784 The timescale of mesopelagic Ba_{xs} as a remineralisation proxy has been reported to be in the order of days to weeks (Dehairs

785 et al., 1997; Jacquet et al., 2015; Planchon et al., 2013). However, the similarity between our results and those from studies

786 conducted during spring and summer strongly suggests a longer timescale. If it was in the order of days to weeks (< 4 weeks),

787 as reported (Dehairs et al., 1997; Jacquet et al., 2015; Planchon et al., 2013), the mesopelagic signal would be expected to be

788 close to the $Ba_{residual}$ value during winter months. The Ba_{xs} signal that we observed in winter is also in agreement with the

789 previous suggestion by Dehairs et al. (1997), that there can be a significant carry over between bloom seasons.

790 The hypothesis that mesopelagic Ba_{xs} has a longer timescale, possibly on an annual scale, was thus tested by investigating a

791 possible link between the integrated mesopelagic Ba_{xs} stock and the corresponding integrated remote sensing PP from the

792 preceding bloom season. In order to do so a SO mesopelagic Ba_{xs} stock dataset was compiled, including all available literature

793 data and data from this study (Table S3). The sample area for the remote sensing PP was determined by assuming a maximum

794 surface current speed of 0.2 m s^{-1} (Ferrari and Nikurashin, 2010) and a particle sinking speed of 50 m d^{-1} (Riebesell et al.,

795 1991), at which surface particles would take up to ~ 20 days to sink down to the bottom of the mesopelagic zone (1000 m).

796 Within these 20 days of particles sinking to the bottom of the mesopelagic zone, a surface current speed of 0.2 m s^{-1} would

797 transport waters 346 km eastward. Using this distance, the dimensions of the sample area were set with the southernmost

798 station (TM1) of this study, where degrees of longitude cover the smallest area. For the sake of consistency this sampling area

799 was applied to all sampling locations of the compilation dataset. The integrated PP was then averaged spatially, positioned 6°

800 upstream longitudinally, and 1° latitudinally centred around each sampled station. Integrated remote sensing PP of the

801 preceding bloom was calculated using the month of September prior to sampling as the start of the bloom. This is in general

802 agreement with previous bloom phenology studies for this region (Thomalla et al., 2011). The PP was integrated up to one

803 month prior to the sampling date of the study, taking into consideration time needed for export, aggregate formation and barite

804 crystal release through remineralisation (~ 1 month). The mesopelagic Ba_{xs} stock was integrated over the Ba_{xs} peak depth range

805 (as identified in each study) in order to link it to the corresponding integrated remote sensing PP. When remote sensing data

06   was limited due to cloud cover and low sunlight during winter months, specifically at the southernmost stations, all available

07   data was used for the duration of the season.

08   Varying timescales were considered between the preceding September up to 1 month prior to sampling, that could influence

09   the relationship between PP and the mesopelagic Ba_{xs} stock. However, the strongest and most significant correlation between

10   the mesopelagic Ba_{xs} stock and integrated remote sensing PP was obtained from the preceding September up to 1 month prior

11   to sampling (Table S4), for the AZ (SPF) (Figure 3a, $R^2 = 0.55$, p-value < 0.05, n = 39) and the SAZ (NPF) (Figure 3b, $R^2 =$

12   0.42, p-value < 0.05, n = 31). The negative correlation observed in the STZ is not significant at a 95 % confidence level (Figure

13   3c, $R^2 = 0.52$, p-value $= 0.10$); however, the limited number of data points may preclude any significance from emerging. The

14   significant positive correlations obtained in the AZ and the SAZ suggest that mesopelagic Ba_{xs} stock can be used as a

15   remineralisation proxy on an annual timescale instead of only a few weeks.
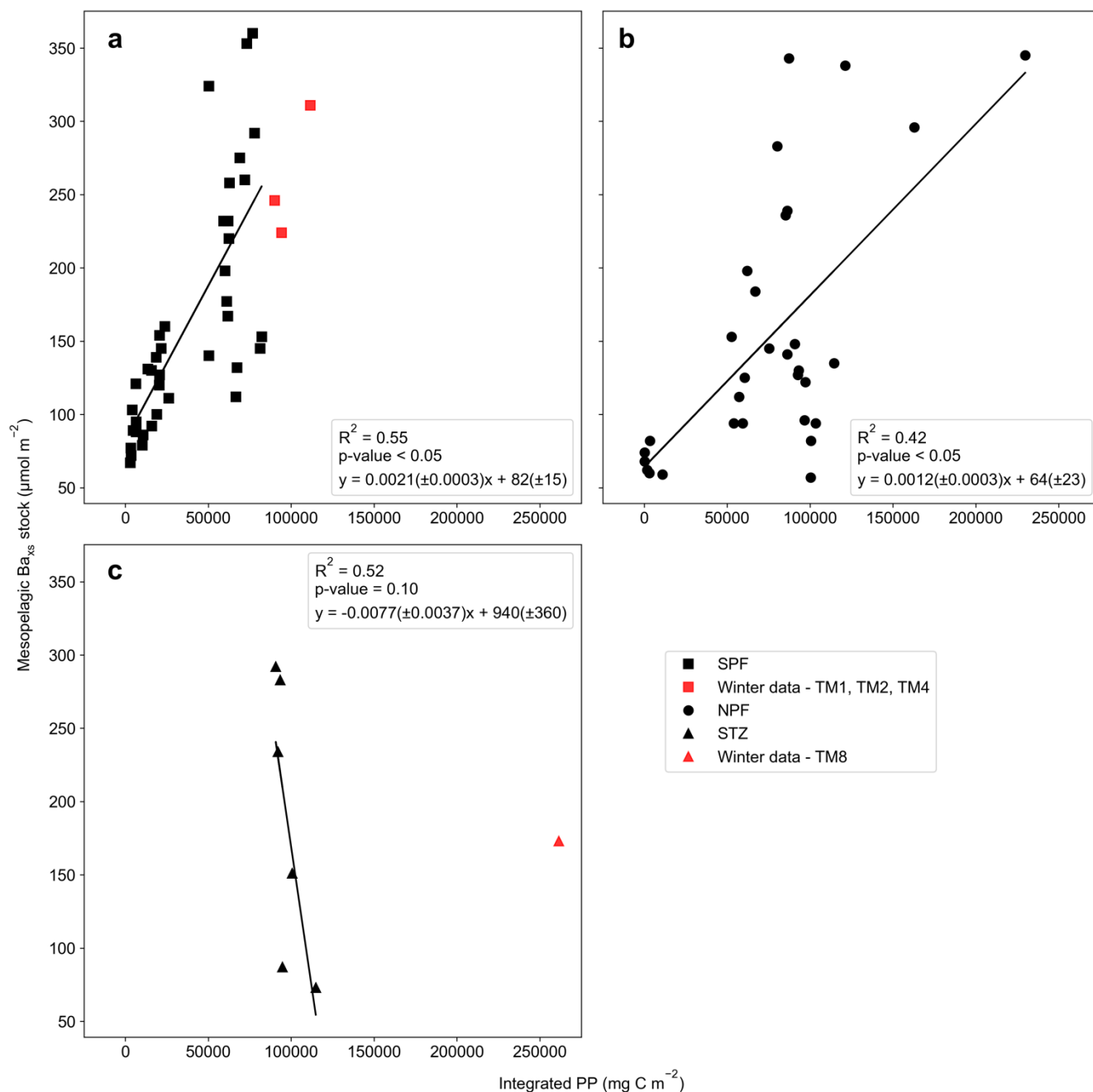
Figure 3: Integrated mesopelagic Ba$_{xs}$ stock plotted against integrated remote sensing PP from the preceding September up to one month prior to sampling, all available literature data and winter data from this study, split into three zones using the Polar Front (PF) to divide the SO; (a) South of the PF (SPF, black squares), (b) North of the PF (NPF, black circles), and (c) Subtropical Zone (STZ, black triangles). Red squares are data points from our winter dataset where there was not sufficient remote sensing PP data to integrate up to 1 month prior to sampling and available data up to 3 months prior to sampling was plotted but not included in the statistical analysis and the red triangle is the STZ station from the winter dataset, which appears to be an outlier, was also excluded from statistical analysis due to the station possibly being strongly influenced by the Agulhas Return Current.

4.3 Environmental factors influencing mesopelagic remineralisation

Welch's t-test was applied to the two regressions to determine a significant difference between zones, NPF and SPF, with a 2-fold, significant difference (t-statistic = 2.24; p-value < 0.05) apparent between the slopes. A combination of variables can influence remineralisation and the mesopelagic Ba_{xs} signal, even more so when considering longer timescales. These variables include phytoplankton community structure, nutrient availability and physical dynamics (Bopp et al., 2013; Buesseler and Boyd, 2009; Cardinal et al., 2005; Jacquet et al., 2008b; Pyle et al., 2018). The Fe-limited SAZ (Ryan-Keogh et al., 2018) and AZ (Viljoen et al., 2018) have generally mixed and seasonally changing assemblages of pico-, nano- and micro-phytoplankton (Eriksen et al., 2018; Gall et al., 2001). Diatoms tend to dominate in silicate-rich waters, SPF (Petrou et al., 2016; Rembauville et al., 2017; Wright et al., 2010), whilst seasonally silicate-limited waters, NPF, favour smaller phytoplankton groups (Freeman et al., 2018; Nissen et al., 2018; Trull et al., 2018). This results in higher surface export efficiency in polar HNLC regions (SPF) due to the presence of these diatoms, when compared to other areas of comparatively higher biomass (Fan et al., 2020; Jacquet et al., 2008b; Planchon et al., 2013). Phytoplankton communities in the STZ are reported to be dominated by prokaryotic picoplankton including cyanobacteria and prochlorophytes (Mendes et al., 2015), utilising regenerated nutrients in the surface mixed layer tending towards diminished surface export efficiency with high concentrations of non-sinking POC (Fan et al., 2020; Planchon et al. 2013).

In previous studies, supply and loss via physical transport has been deemed negligible relative to decay and loss via production, due to minimal advection and diffusion gradients observed on the timescale of days to weeks, thereby assuming these processes have minimal impact on the mesopelagic signal (Dehairs et al., 1997; Planchon et al., 2013; Rutgers van der Loeff et al., 2011). It has, however, been observed that features such as mesoscale eddies can have an effect on Ba_{xs} distribution by influencing particle patterns on a broad spatial scale, homogenizing mesopelagic remineralisation signals by causing relatively flat profiles or shallower remineralisation peaks (Buesseler et al., 2005; Jacquet et al., 2008b). These observations indicate that the mesopelagic Ba_{xs} signal could be influenced by physical processes deeming it necessary to consider these factors when looking at longer timescales (Rutgers van der Loeff et al., 2011, Planchon et al., 2013). The region of our winter study is known for being a mesoscale eddy hotspot due to the South-West Indian Ridge (Ansorge et al., 2013); therefore, eddies could have influenced the mesopelagic Ba_{xs} signal we observed along the transect of this study as well as in other studies throughout the SO. However, the strong significant correlations we observe south of the STF seem to indicate that physical transport variability is not a dominant process affecting the mesopelagic Ba_{xs} signal. The STZ is on the contrary characteristic of extremely dynamic submesoscale activity due to the Agulhas return current, which may be a crucial factor masking a significant relationship from being observed.

4.4 Mesopelagic POC remineralisation

Estimated POC remineralisation fluxes along our transect were on the upper end of the range of fluxes from previous studies, but within the same order of magnitude for the SO as estimated from spring to autumn (Cardinal et al., 2005; Jacquet et al.,

56 2011, 2015; Planchon et al., 2013). Heterogeneity has been observed in mesopelagic remineralisation fluxes across regions of

57 variable conditions and due to seasonal advancement of the bloom (Jacquet et al., 2011, 2015; Planchon et al., 2013). Estimated

58 mesopelagic POC remineralisation has been reported to account for a significant fraction of exported carbon in the PFZ and

59 southwards, from 31 to 97 %, from spring to summer, whereas it only accounts for ~ 50% in the SAZ and SAF, during summer

60 (Cardinal et al., 2005). As the bloom season progresses, more efficient remineralisation rates have been reported in multiple

61 studies (Cardinal et al., 2005; Jacquet et al., 2011; Planchon et al., 2013). However, during late summer as the bloom declines,

62 observations indicate an inefficient BCP due to enhanced surface nutrient recycling, leading to a decrease in surface POC

63 export (Planchon et al., 2013). Seasonal variation is reported to be more pronounced northwards within the SO with the least

64 variation observed in the southern ACC (Dehairs et al., 1997; Planchon et al., 2013).

65 When determining the % POC remineralised against the integrated remote sensing PP, there was no significant difference

66 between the zones. This indicates that even though there is a significant difference in the response of the mesopelagic Ba_{xs}

67 stock to integrated remote sensing PP between the NPF and SPF regions, as a result of the varying impact of the environmental

68 drivers, this significant difference is not observed in the % POC remineralised. This highlights the difference in surface export

69 efficiency between the two zones forced by different environmental factors, positively or negatively to varying degrees. High

70 productivity, low export (HPLE) regimes are characteristic of large areas of the subpolar SO, these regimes can largely be

71 explained by surface POC accumulation caused by non-sinking particles, tending towards less efficient export of smaller cells,

72 whereas the polar SO has not been identified as a HPLE regime (Fan et al., 2020). It cannot, however, be discounted that $C:O_2$

73 ratio deviations from the Redfield ratio could introduce errors in the estimation of POC remineralisation fluxes, highlighting

74 the need to better constrain the factors and processes governing surface export and mesopelagic remineralisation.

75 The low mean % POC remineralised values (SPF; 19 ± 15 %, n = 39 and NPF; 25 ± 58 %, n = 31; mean ± SD) observed for

76 studies in the compilation dataset (Table S1), are comparable to surface export efficiency observations in this region. It has

77 indeed been reported that more than 90 % of the POC pool is retained in the surface ocean (Baker et al., 2017; Riley et al.,

78 2012), causing surface accumulation which is hypothesized to have a large impact on carbon export efficiency in the SO on

79 regional and seasonal timescales (Fan et al., 2020). Linking cumulative PP to Ba_{xs}, coupled with the added influence of physical

80 dynamics affecting surface export efficiencies, along longer timescales, could give better estimates of true export and

81 remineralisation signals within the SO on an annual and basin scale.

5 Conclusions

83 The expected decline of the mesopelagic Ba_{xs} signal to background values during winter was not observed in this study,

84 supporting our hypothesis that this remineralisation proxy has a longer timescale than previously reported. The absolute decline

85 might never be achieved due to the cumulative behaviour of Ba_{xs} and ongoing remineralisation and barite precipitation. Early

86 winter Ba_{xs} distributions were similar in magnitude and exhibited the same relationship with σ_θ and dissolved O_2 gradients as

87 observed in summer, indicating that processes controlling this signal in summer are still driving the signal in early winter. A

488 similar latitudinal trend was also still apparent during early winter as observed in summer, with higher values NPF, where PP

489 is higher and bloom seasons are longer (Thomalla et al., 2011), indicative of the cumulative behaviour this proxy exhibits as

490 the season advances. The difference in background values of saturated versus unsaturated deep waters was also not apparent

491 in our data where we detected no significant difference between values NPF and SPF. It is, however, possible that the most

492 accurate background signal can be expected at the end of winter, prior to bloom initiation, during August, once remineralisation

493 processes have been exhausted.

494 Significant positive correlations between integrated remote sensing PP and mesopelagic Ba_{xs} stock suggest an annual timescale

495 and/or that continuous remineralisation within the mesopelagic zone, well after bloom termination, is sustained at least during

496 the first month of winter. A significant difference in the mesopelagic Ba_{xs} response to PP between zones, NPF and SPF, is

497 indicative of the contrast in export efficiencies. HPLE regimes are characteristic NPF where surface POC accumulation has a

498 significant impact on the efficiency of surface export, however, this is not the case SPF (Fan et al., 2020; Figure 4). No

499 significant difference in % POC remineralised between the zones is also evidence of the difference in surface export

500 efficiencies between the two regimes, as it is not controlled by the magnitude of PP. Remineralisation SPF where the

501 phytoplankton community structure is generally dominated by diatoms, bulk surface export and mesopelagic remineralisation

502 matches the magnitude observed NPF, despite much lower PP and a shorter bloom season (Figure 4). Strong correlations

503 observed between integrated remote sensing PP and mesopelagic Ba_{xs} stock indicate that physical processes do not seem to

504 dominate the mesopelagic signal on an annual scale, within the SO. The longer timescale of Ba_{xs} and the cumulative behaviour

505 of this proxy in the mesopelagic zone make it possible to use Ba_{xs} on an annual scale for the estimation of POC remineralisation

506 fluxes throughout the SO and to better understand how variable environmental factors influence these processes on a basin

507 scale.
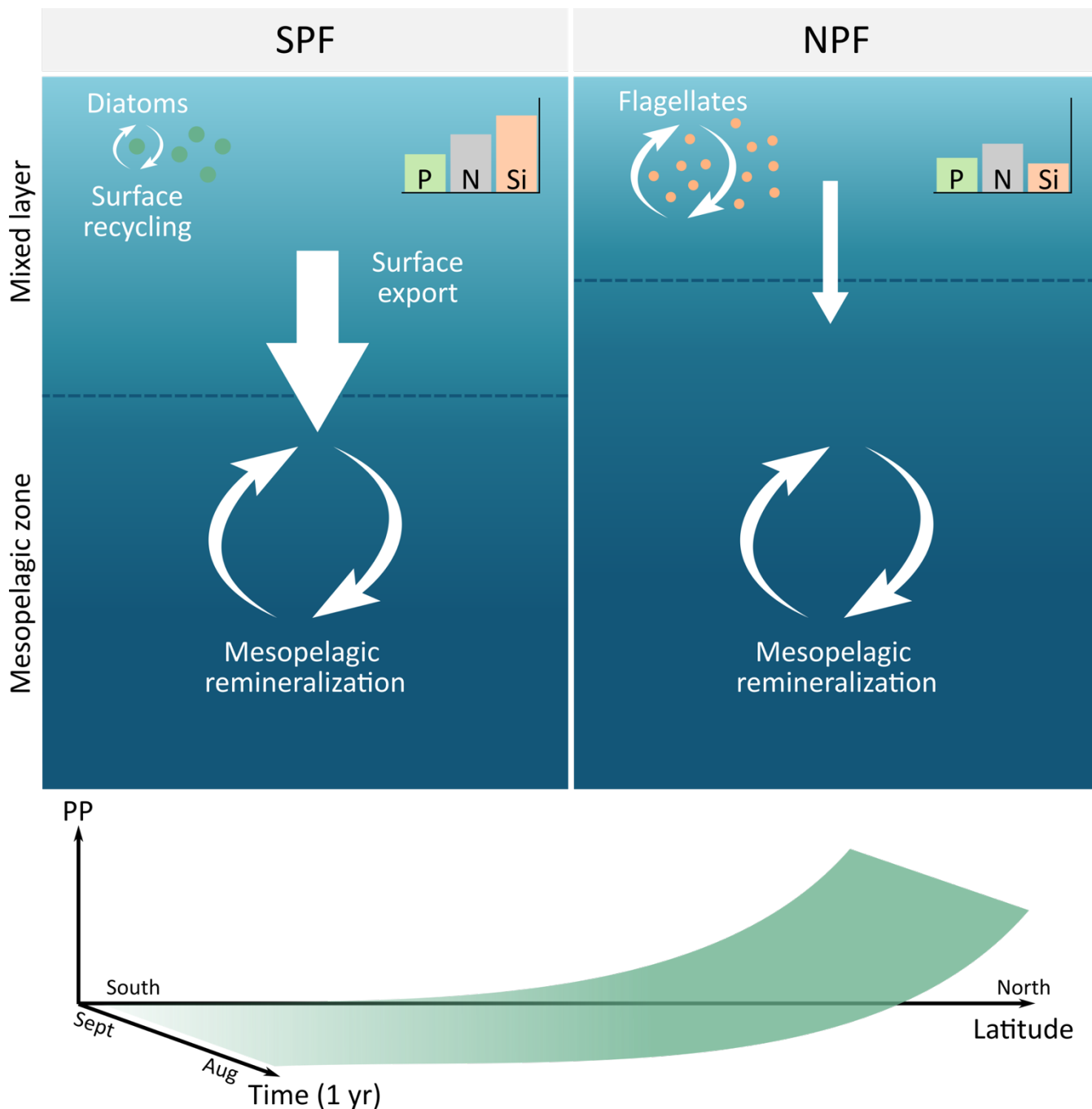
Figure 4: Schematic diagram highlighting the contrast between the two zones, SPF and NPF. SPF is diatom dominated, high concentrations of macronutrients, low surface layer recycling and more efficient surface export despite low PP. NPF is flagellate dominated, tending towards Si limitation, increased surface recycling and less efficient surface export, resulting in comparable mesopelagic remineralisation despite higher PP in the NPF zone, indicative of a high productivity, low export regime whereas SPF is not.

6 Author contribution

This study was conceptualised by N.R.vH, H.P, G.S and E.B. Formal analysis, investigation and validation of data was carried out by N.R.vH, H.P, G.S, T.J.R-K and T.N.M. N.R.vH and T.J.R-K contributed towards the visualisation of the data. H.P, G.S, T.N.M, A.R and E.B contributed towards supervision and resources. Funding was acquired by N.R.vH, T.N.M, A.R and E.B. All authors contributed towards writing, reviewing and editing of the final manuscript.

7 Acknowledgments

This work was supported by the ISblue project, Interdisciplinary graduate school for the blue planet (ANR-17-EURE-0015) and co-funded by a grant from the French government under the program "Investissements d'Avenir". International collaboration was made possible by funding received by the French-South African National Research Foundation (NRF) Collaboration (PROTEA; FSTR180418322331), NRF funding (SNA170518231343 and UID 110715) including funding from South African Department of Science and Technology, French Ministry of National Education, Higher Education and Research, and the French Ministry of Foreign Affairs and International Development. We would like to thank the captain and crew of the R/V *SA Agulhas II* for their invaluable efforts, as well as all the research participants who assisted our fieldwork. Thanks to Prof. I Ansorge, Dr M du Plessis and Dr E Portela for their assistance with water mass identification, Dr N Llopis Monferrer for creating the schematic diagram and Dr Jeandel for her invaluable expert insight.

8 Data availability

Underlying data are made available online at ftp://socco.chpc.ac.za/VanHorsten_etal_2021/

9 References

Anilkumar, N. and Sabu, P.: Physical process influencing the ecosystem of the indian sector of southern ocean-An overview, Proc. Indian Natl. Sci. Acad., 83(2), 363–376, doi:10.16943/ptinsa/2017/48960, 2017.

Ansorge, I. J., Jackson, J. M., Reid, K., Durgadoo, J. V, Swart, S. and Eberenz, S.: Evidence of a southward eddy corridor in the South-West Indian ocean, Deep. Res. Part II Top. Stud. Oceanogr., 119, 69–76, doi:10.1016/j.dsr2.2014.05.012, 2015.

Armstrong, R. A., Peterson, M. L., Lee, C. and Wakeham, S. G.: Settling velocity spectra and the ballast ratio hypothesis, Deep. Res. Part II Top. Stud. Oceanogr., 56(18), 1470–1478, doi:10.1016/j.dsr2.2008.11.032, 2009.

Baker, C. A., Henson, S. A., Cavan, E. L., Giering, S. L. C., Yool, A., Gehlen, M., Belcher, A., Riley, J. S., Smith, H. E. K. and Sanders, R.: Slow-sinking particulate organic carbon in the Atlantic Ocean: Magnitude, flux, and potential controls, Global Biogeochem. Cycles, 31(7), 1051–1065, doi:10.1002/2017GB005638, 2017.

Behrenfeld, M. J., Boss, E., Siegel, D. A. and Shea, D. M.: Carbon-based ocean productivity and phytoplankton physiology from space, Global Biogeochem. Cycles, 19(1), 1–14, doi:10.1029/2004GB002299, 2005.

Bishop, J. K. B.: The barite-opal-organic carbon association in oceanic particulate matter, Nature, 332(6162), 341–343, doi:10.1038/332341a0, 1988.

Bopp, L., Resplandy, L., Orr, J. C., Doney, S. C., Dunne, J. P., Gehlen, M., Halloran, P., Heinze, C., Ilyina, T., Séférian, R., Tjiputra, J. and Vichi, M.: Multiple stressors of ocean ecosystems in the 21st century: Projections with CMIP5 models, Biogeosciences, 10(10), 6225–6245, doi:10.5194/bg-10-6225-2013, 2013.

Boyd, P. W., Claustre, H., Levy, M., Siegel, D. A. and Weber, T.: Multi-faceted particle pumps drive carbon sequestration in the ocean, Nature, 568(7752), 327–335, doi:10.1038/s41586-019-1098-2, 2019.

Broecker, W. S., Takahashi, T. and Takahashi, T.: Sources and flow patterns of deep-ocean waters as deduced from potential temperature, salinity, and initial phosphate concentration, J. Geophys. Res. Ocean., 90(C4), 6925–6939, doi:10.1029/JC090iC04p06925, 1985.

Buesseler, K. O.: The decoupling of production and particulate export in the surface ocean, Global Biogeochem. Cycles, 12(2), 297–310, doi:10.1029/97GB03366, 1998.

Buesseler, K. O., Andrews, J. E., Pike, S. M., Charette, M. A., Goldson, L. E., Brzezinski, M. A. and Lance, V. P.: Particle export during the Southern Ocean Iron Experiment (SOFeX), Limnol. Oceanogr., 50(1), 311–327, doi:10.4319/lo.2005.50.1.0311, 2005.

Buesseler, K. O. and Boyd, P. W.: Shedding light on processes that control particle export and flux attenuation in the twilight zone of the open ocean, Limnol. Oceanogr., 54(4), 1210–1232, doi:10.4319/lo.2009.54.4.1210, 2009.

Cardinal, D., Dehairs, F., Cattaldo, T. and André, L.: Geochemistry of suspended particles in the Subantarctic and Polar Frontal zones south of Australia: Constraints on export and advection processes, J. Geophys. Res. Ocean., 106(C12), 31637–31656, doi:10.1029/2000JC000251, 2001.

Cardinal, D., Savoye, N., Trull, T. W., André, L., Kopczynska, E. E. and Dehairs, F.: Variations of carbon remineralisation in the Southern Ocean illustrated by the Baxs proxy, Deep. Res. Part I Oceanogr. Res. Pap., 52(2), 355–370, doi:10.1016/j.dsr.2004.10.002, 2005.

Cutter, G., Casciotti, K., Croot, P., Geibert, W., Heimbürger, L.-E., Lohan, M., Planquette, H. and van de Flierdt, T.: Sampling and Sample-handling Protocols for GEOTRACES Cruises. Version 3, 139pp. & Appendices [online] Available from: http://www.geotraces.org/images/stories/documents/intercalibration/Cookbook.pdf, 2017.

de Boyer Montégut, C., Madec, G., Fischer, A. S., Lazar, A. and Iudicone, D.: Mixed layer depth over the global ocean: An examination of profile data and a profile-based climatology, J. Geophys. Res. C Ocean., 109(12), 1–20, doi:10.1029/2004JC002378, 2004.

Dehairs, F., Shopova, D., Ober, S., Veth, C. and Goeyens, L.: Particulate barium stocks and oxygen consumption in the Southern Ocean mesopelagic water column during spring and early summer: Relationship with export production, Deep. Res. Part II Top. Stud. Oceanogr., 44(1–2), 497–516, doi:10.1016/S0967-0645(96)00072-0, 1997.

DeVries, T. and Weber, T.: The export and fate of organic matter in the ocean: New constraints from combining satellite and oceanographic tracer observations, Global Biogeochem. Cycles, 31(3), 535–555, doi:10.1002/2016GB005551, 2017.

Ducklow, H. W., Steinberg, D. K. and Buesseler, K. O.: Upper ocean carbon export and the biological pump, Oceanography, 14(SPL.ISS. 4), 50–58, doi:10.5670/oceanog.2001.06, 2001.

Dymond, J., Suess, E. and Lyle, M.: Barium in Deep-Sea Sediment: A Geochemical Proxy for Paleoproductivity, Paleoceanography, 7(2), 163–181, doi:10.1029/92PA00181, 1992.

Ehrhardt, M. (Manfred), Grasshoff, K., Kremling, K. (Klaus) and Almgren, T., Eds.: Methods of seawater analysis / edited by K. Grasshoff, M. Ehrhardt, K. Kremling ; with contributions by T. Almgren ... [et al.], Verlag Chemie, Weinheim., 1983.

Eriksen, R., Trull, T. W., Davies, D., Jansen, P., Davidson, A. T., Westwood, K. and Van Den Enden, R.: Seasonal succession of phytoplankton community structure from autonomous sampling at the Australian Southern Ocean Time Series (SOTS) observatory, Mar. Ecol. Prog. Ser., 589, 13–21, doi:10.3354/meps12420, 2018.

Fan, G., Han, Z., Ma, W., Chen, S., Chai, F., Mazloff, M. R., Pan, J. and Zhang, H.: Southern Ocean carbon export efficiency in relation to temperature and primary productivity, Sci. Rep., 10(1), 1–11, doi:10.1038/s41598-020-70417-z, 2020.

Ferrari, R. and Nikurashin, M.: Suppression of eddy diffusivity across jets in the Southern Ocean, J. Phys. Oceanogr., 40(7), 1501–1519, doi:10.1175/2010JPO4278.1, 2010.

Freeman, N. M., Lovenduski, N. S., Munro, D. R., Krumhardt, K. M., Lindsay, K., Long, M. C. and Maclennan, M.: The Variable and Changing Southern Ocean Silicate Front: Insights from the CESM Large Ensemble, Global Biogeochem. Cycles, 32(5), 752–768, doi:10.1029/2017GB005816, 2018.

Friedlingstein, P., Jones, M. W., O'Sullivan, M., Andrew, R. M., Hauck, J., Peters, G. P., Peters, W., Pongratz, J., Sitch, S., Le Quéré, C., Bakker, D. C. E., Canadell, J. G., Ciais, P., Jackson, R. B., Anthoni, P., Barbero, L., Bastos, A., Bastrikov, V., Becker, M., Bopp, L., Buitenhuis, E., Chandra, N., Chevallier, F., Chini, L. P., Currie, K. I., Feely, R. A., Gehlen, M., Gilfillan, D., Gkritzalis, T., Goll, D. S., Gruber, N., Gutekunst, S., Harris, I., Haverd, V., Houghton, R. A., Hurtt, G., Ilyina, T., Jain, A. K., Joetzjer, E., Kaplan, J. O., Kato, E., Klein Goldewijk, K., Korsbakken, J. I., Landschützer, P., Lauvset, S. K., Lefèvre, N., Lenton, A., Lienert, S., Lombardozzi, D., Marland, G., McGuire, P. C., Melton, J. R., Metzl, N., Munro, D. R., Nabel, J. E. M. S., Nakaoka, S.-I., Neill, C., Omar, A. M., Ono, T., Peregon, A., Pierrot, D., Poulter, B., Rehder, G., Resplandy, L., Robertson, E., Rödenbeck, C., Séférian, R., Schwinger, J., Smith, N., Tans, P. P., Tian, H., Tilbrook, B., Tubiello, F. N., van der Werf, G. R., Wiltshire, A. J. and Zaehle, S.: Global Carbon Budget 2019, Earth Syst. Sci. Data, 11(4), 1783–1838, doi:10.5194/essd-11-1783-2019, 2019.

Gall, M. P., Boyd, P. W., Hall, J., Safi, K. A. and Chang, H.: Phytoplankton processes. Part 1: Community structure during the Southern Ocean Iron RElease Experiment (SOIREE), Deep. Res. Part II Top. Stud. Oceanogr., 48(11–12), 2551–2570, doi:10.1016/S0967-0645(01)00008-X, 2001.

Gill, A. E.: Atmosphere-ocean dynamics, NEW YORK, U.S.A., ACADEMIC PRESS INC., 1982.

Gregor, L., Lebehot, A. D., Kok, S. and Scheel Monteiro, P. M.: A comparative assessment of the uncertainties of global surface ocean CO2 estimates using a machine-learning ensemble (CSIR-ML6 version 2019a)-Have we hit the wall?, Geosci. Model Dev., 12(12), 5113–5136, doi:10.5194/gmd-12-5113-2019, 2019.

Gruber, N., Landschützer, P. and Lovenduski, N. S.: The variable southern ocean carbon sink, Ann. Rev. Mar. Sci., 11(September), 159–186, doi:10.1146/annurev-marine-121916-063407, 2019.

Honjo, S., Eglinton, T. I., Taylor, C. D., Ulmer, K. M., Sievert, S. M., Bracher, A., German, C. R., Edgcomb, V., Francois, R., Deboraiglesias-Rodriguez, M., Van Mooy, B. and Repeta, D. J.: Understanding the role of the biological pump in the global carbon cycle: An imperative for ocean science, Oceanography, 27(3), 10–16, doi:10.5670/oceanog.2014.78, 2014.

Ito, T., Follows, M. J. and Boyle, E. A.: Is AOU a good measure of respiration in the oceans?, Geophys. Res. Lett., 31(17), 1–4, doi:10.1029/2004GL020900, 2004.

Jacquet, S. H. M., Dehairs, F., Cardinal, D., Navez, J. and Delille, B.: Barium distribution across the Southern Ocean frontal system in the Crozet-Kerguelen Basin, Mar. Chem., 95(3–4), 149–162, doi:10.1016/j.marchem.2004.09.002, 2005.

Jacquet, S. H. M., Dehairs, F., Dumont, I., Becquevort, S., Cavagna, A. J. and Cardinal, D.: Twilight zone organic carbon remineralization in the Polar Front Zone and Subantarctic Zone south of Tasmania, Deep. Res. Part II Top. Stud. Oceanogr., 58(21–22), 2222–2234, doi:10.1016/j.dsr2.2011.05.029, 2011.

Jacquet, S. H. M., Dehairs, F., Elskens, M., Savoye, N. and Cardinal, D.: Barium cycling along WOCE SR3 line in the Southern Ocean, Mar. Chem., 106(1-2 SPEC. ISS.), 33–45, doi:10.1016/j.marchem.2006.06.007, 2007.

Jacquet, S. H. M., Dehairs, F., Lefèvre, D., Cavagna, A. J., Planchon, F., Christaki, U., Monin, L., André, L., Closset, I. and Cardinal, D.: Early spring mesopelagic carbon remineralization and transfer efficiency in the naturally iron-fertilized Kerguelen area, Biogeosciences, 12(6), 1713–1731, doi:10.5194/bg-12-1713-2015, 2015.

Jacquet, S. H. M., Dehairs, F., Savoye, N., Obernosterer, I., Christaki, U., Monnin, C. and Cardinal, D.: Mesopelagic organic carbon remineralization in the Kerguelen Plateau region tracked by biogenic particulate Ba, Deep. Res. Part II Top. Stud. Oceanogr., 55(5–7), 868–879, doi:10.1016/j.dsr2.2007.12.038, 2008a.

Jacquet, S. H. M., Savoye, N., Dehairs, F., Strass, V. H. and Cardinal, D.: Mesopelagic carbon remineralization during the European Iron Fertilization Experiment, Global Biogeochem. Cycles, 22(1), 1–9, doi:10.1029/2006GB002902, 2008b.

Jochum, K. P., Nohl, U., Herwig, K., Lammel, E., Stoll, B. and Hofmann, A. W.: GeoReM: A new geochemical database for reference materials and isotopic standards, Geostand. Geoanalytical Res., 29(3), 333–338, doi:10.1111/j.1751-908x.2005.tb00904.x, 2005.

Kokoska, S. and Zwillinger, D.: CRC Standard Probability and Statistics Tables and Formulae, Student Edition., 2000.

Lam, P. J. and Bishop, J. K. B.: High biomass, low export regimes in the Southern Ocean, Deep. Res. Part II Top. Stud. Oceanogr., 54(5–7), 601–638, doi:10.1016/j.dsr2.2007.01.013, 2007.

Le Moigne, F. A. C.: Pathways of Organic Carbon Downward Transport by the Oceanic Biological Carbon Pump, Front. Mar. Sci., 6, doi:10.3389/fmars.2019.00634, 2019.

Legeleux, F. and Reyss, J. L.: 228Ra/226Ra activity ratio in oceanic settling particles: Implications regarding the use of barium as a proxy for paleoproductivity reconstruction, Deep. Res. Part I Oceanogr. Res. Pap., 43(11–12), 1857–1863, doi:10.1016/S0967-0637(96)00086-6, 1996.

Lemaitre, N., Planquette, H., Planchon, F., Sarthou, G., Jacquet, S., García-Ibáñez, M. I., Gourain, A., Cheize, M., Monin, L., André, L., Laha, P., Terryn, H. and Dehairs, F.: Particulate barium tracing of significant mesopelagic carbon remineralisation in the North Atlantic, Biogeosciences, 15(8), 2289–2307, doi:10.5194/bg-15-2289-2018, 2018.

Marsay, C. M., Sanders, R. J., Henson, S. A., Pabortsava, K., Achterberg, E. P. and Lampitt, R. S.: Attenuation of sinking particulate organic carbon flux through the mesopelagic ocean, Proc. Natl. Acad. Sci. U. S. A., 112(4), 1089–1094, doi:10.1073/pnas.1415311112, 2015.

Mendes, C. R. B., Kerr, R., Tavano, V. M., Cavalheiro, F. A., Garcia, C. A. E., Gauns Dessai, D. R. and Anilkumar, N.: Cross-front phytoplankton pigments and chemotaxonomic groups in the Indian sector of the Southern Ocean, Deep. Res. Part II Top. Stud. Oceanogr., 118, 221–232, doi:10.1016/j.dsr2.2015.01.003, 2015.

Monnin, C., Jeandel, C., Cattaldo, T. and Dehairs, F.: The marine barite saturation state of the world's oceans, Mar. Chem., 65(3–4), 253–261, doi:10.1016/S0304-4203(99)00016-X, 1999.

Barbur, V. A., Montgomery, D. C. and Peck, E. A.: Introduction to Linear Regression Analysis., Stat., 43(2), 339, doi:10.2307/2348362, 1994.

Nissen, C., Vogt, M., Münnich, M., Gruber, N. and Haumann, F. A.: Factors controlling coccolithophore biogeography in the Southern Ocean, Biogeosciences, 15(22), 6997–7024, doi:10.5194/bg-15-6997-2018, 2018.

Orsi, A. H., Whitworth, T. and Nowlin, W. D.: On the meridional extent and fronts of the Antarctic Circumpolar Current, Deep. Res. Part I, 42(5), 641–673, doi:10.1016/0967-0637(95)00021-W, 1995.

Passow, U. and Carlson, C. A.: The biological pump in a high CO2 world, Mar. Ecol. Prog. Ser., 470(2), 249–271, doi:10.3354/meps09985, 2012.

Petrou, K., Kranz, S. A., Trimborn, S., Hassler, C. S., Ameijeiras, S. B., Sackett, O., Ralph, P. J. and Davidson, A. T.: Southern Ocean phytoplankton physiology in a changing climate, J. Plant Physiol., 203, 135–150, doi:https://doi.org/10.1016/j.jplph.2016.05.004, 2016.

Planchon, F., Cavagna, A. J., Cardinal, D., André, L. and Dehairs, F.: Late summer particulate organic carbon export and twilight zone remineralisation in the Atlantic sector of the Southern Ocean, Biogeosciences, 10(2), 803–820, doi:10.5194/bg-10-803-2013, 2013.

Planquette, H. and Sherrell, R. M.: Sampling for particulate trace element determination using water sampling bottles: Methodology and comparison to in situ pumps, Limnol. Oceanogr. Methods, 10(5), 367–388, doi:10.4319/lom.2012.10.367, 2012.

Pyle, K. M., Hendry, K. R., Sherrell, R. M., Legge, O., Hind, A. J., Bakker, D., Venables, H. and Meredith, M. P.: Oceanic fronts control the distribution of dissolved barium in the Southern Ocean, Mar. Chem., 204(July), 95–106, doi:10.1016/j.marchem.2018.07.002, 2018.

Rembauville, M., Briggs, N., Ardyna, M., Uitz, J., Catala, P., Penkerc'h, C., Poteau, A., Claustre, H. and Blain, S.: Plankton Assemblage Estimated with BGC-Argo Floats in the Southern Ocean: Implications for Seasonal Successions and Particle Export, J. Geophys. Res. Ocean., 122(10), 8278–8292, doi:10.1002/2017JC013067, 2017.

Riebesell, U.: Particle aggregation during a diatom bloom. II. Biological aspects, Mar. Ecol. Prog. Ser., 69(3), 281–291, doi:10.3354/meps069281, 1991.

Riley, J. S., Sanders, R., Marsay, C., Le Moigne, F. A. C., Achterberg, E. P. and Poulton, A. J.: The relative contribution of fast and slow sinking particles to ocean carbon export, Global Biogeochem. Cycles, 26(1), 1–10, doi:10.1029/2011GB004085, 2012.

Rio, M. H., Guinehut, S. and Larnicol, G.: New CNES-CLS09 global mean dynamic topography computed from the combination of GRACE data, altimetry, and in situ measurements, J. Geophys. Res. Ocean., 116(7), 1–25, doi:10.1029/2010JC006505, 2011.

Robinson, C., Steinberg, D. K., Anderson, T. R., Arístegui, J., Carlson, C. A., Frost, J. R., Ghiglione, J. F., Hernández-León, S., Jackson, G. A., Koppelmann, R., Quéguiner, B., Ragueneau, O., Rassoulzadegan, F., Robison, B. H., Tamburini, C., Tanaka, T., Wishner, K. F. and Zhang, J.: Mesopelagic zone ecology and biogeochemistry - A synthesis, Deep. Res. Part II Top. Stud. Oceanogr., 57(16), 1504–1518, doi:10.1016/j.dsr2.2010.02.018, 2010.

Rosengard, S. Z., Lam, P. J., Balch, W. M., Auro, M. E., Pike, S., Drapeau, D. and Bowler, B.: Carbon export and transfer to depth across the Southern Ocean Great Calcite Belt, Biogeosciences, 12(13), 3953–3971, doi:10.5194/bg-12-3953-2015, 2015.

Rutgers van der Loeff Michiel, M., Cai, P. H., Stimac, I., Bracher, A., Middag, R., Klunder, M. B. and van Heuven, S. M. A. C.: 234Th in surface waters: Distribution of particle export flux across the Antarctic Circumpolar Current and in the Weddell Sea during the GEOTRACES expedition ZERO and DRAKE, Deep. Res. Part II Top. Stud. Oceanogr., 58(25–26), 2749–2766, doi:10.1016/j.dsr2.2011.02.004, 2011.

Ryan-Keogh, T. J., Thomalla, S. J., Mtshali, T. N., Van Horsten, N. R. and Little, H. J.: Seasonal development of iron limitation in the sub-Antarctic zone, Biogeosciences, 15(14), 4647–4660, doi:10.5194/bg-15-4647-2018, 2018.

Sarmiento, J., & Gruber, N. Ocean Biogeochemical Dynamics, Princeton University Press, Princeton, Oxford doi:10.2307/j.ctt3fgxqx, 2006.

Sathyendranath, S., Brewin, R. J. W., Brockmann, C., Brotas, V., Calton, B., Chuprin, A., Cipollini, P., Couto, A. B., Dingle, J., Doerffer, R., Donlon, C., Dowell, M., Farman, A., Grant, M., Groom, S., Horseman, A., Jackson, T., Krasemann, H., Lavender, S., Martinez-Vicente, V., Mazeran, C., Mélin, F., Moore, T. S., Müller, D., Regner, P., Roy, S., Steele, C. J., Steinmetz, F., Swinton, J., Taberner, M., Thompson, A., Valente, A., Zühlke, M., Brando, V. E., Feng, H., Feldman, G., Franz, B. A., Frouin, R., Gould, R. W., Hooker, S. B., Kahru, M., Kratzer, S., Mitchell, B. G., Muller-Karger, F. E., Sosik, H. M., Voss, K. J., Werdell, J. and Platt, T.: An ocean-colour time series for use in climate studies: The experience of the ocean-colour climate change initiative (OC-CCI), Sensors (Switzerland), 19(19), doi:10.3390/s19194285, 2019.

Schlitzer, R.: Carbon export fluxes in the Southern Ocean: Results from inverse modeling and comparison with satellite-based estimates, Deep. Res. Part II Top. Stud. Oceanogr., 49(9–10), 1623–1644, doi:10.1016/S0967-0645(02)00004-8, 2002.

Shopova, D., Dehairs, F. and Baeyens, W.: A simple model of biogeochemical element distribution in the oceanic water column, J. Mar. Syst., 6(4), 331–344, doi:10.1016/0924-7963(94)00032-7, 1995.

Sigman, D. M., Hain, M. P. and Haug, G. H.: The polar ocean and glacial cycles in atmospheric CO2 concentration, Nature, 466(7302), 47–55, doi:10.1038/nature09149, 2010.

Sternberg, E., Tang, D., Ho, T. Y., Jeandel, C. and Morel, F. M. M.: Barium uptake and adsorption in diatoms, Geochim. Cosmochim. Acta, 69(11), 2745–2752, doi:10.1016/j.gca.2004.11.026, 2005.

Swart, S., Speich, S., Ansorge, I. J. and Lutjeharms, J. R. E.: An altimetry-based gravest empirical mode south of Africa: 1. Development and validation, J. Geophys. Res. Ocean., 115(3), 1–19, doi:10.1029/2009JC005299, 2010.

Takahashi, T., Sweeney, C., Hales, B., Chipman, D. W., Goddard, J. G., Newberger, T., Iannuzzi, R. A. and Sutherland, S. C.: The changing carbon cycle in the southern ocean, Oceanography, 25(3), 26–37, doi:10.5670/oceanog.2012.71, 2012.

Taylor, S. R. and McLennan, S. M.: The continental crust: Its composition and evolution, Blackwell Scientific Pub., Palo Alto, CA, United States. [online] Available from: https://www.osti.gov/biblio/6582885, 1985.

Thomalla, S. J., Fauchereau, N., Swart, S. and Monteiro, P. M. S.: Regional scale characteristics of the seasonal cycle of chlorophyll in the Southern Ocean, Biogeosciences, 8(10), 2849–2866, doi:10.5194/bg-8-2849-2011, 2011.

Trull, T. W., Passmore, A., Davies, D. M., Smit, T., Berry, K. and Tilbrook, B.: Distribution of planktonic biogenic carbonate organisms in the Southern Ocean south of Australia: A baseline for ocean acidification impact assessment, Biogeosciences, 15(1), 31–49, doi:10.5194/bg-15-31-2018, 2018.

Twining, B. S., Nodder, S. D., King, A. L., Hutchins, D. A., LeCleir, G. R., DeBruyn, J. M., Maas, E. W., Vogt, S., Wilhelm, S. W. and Boyd, P. W.: Differential remineralization of major and trace elements in sinking diatoms, Limnol. Oceanogr., 59(3), 689–704, doi:https://doi.org/10.4319/lo.2014.59.3.0689, 2014.

van Beek, P., François, R., Conte, M., Reyss, J. L., Souhaut, M. and Charette, M.: 228Ra/226Ra and 226Ra/Ba ratios to track barite formation and transport in the water column, Geochim. Cosmochim. Acta, 71(1), 71–86, doi:10.1016/j.gca.2006.07.041, 2007.

Viljoen, J. J., Philibert, R., Van Horsten, N., Mtshali, T., Roychoudhury, A. N., Thomalla, S. and Fietz, S.: Phytoplankton response in growth, photophysiology and community structure to iron and light in the Polar Frontal Zone and Antarctic waters, Deep. Res. Part I Oceanogr. Res. Pap., 141(September), 118–129, doi:10.1016/j.dsr.2018.09.006, 2018.

Wright, S. W., van den Enden, R. L., Pearce, I., Davidson, A. T., Scott, F. J. and Westwood, K. J.: Phytoplankton community structure and stocks in the Southern Ocean (30-80°E) determined by CHEMTAX analysis of HPLC pigment signatures, Deep. Res. Part II Top. Stud. Oceanogr., 57(9–10), 758–778, doi:10.1016/j.dsr2.2009.06.015, 2010.